Early Development Of Stress Corrosion Cracks At The Grain Scale: Incomplete Random Tessellation Model

Leon Cizelj, Marko Kovač
"Jožef Stefan" Institute, Reactor Engineering Division, Ljubljana, Slovenia

ABSTRACT

Computational algorithms aiming at modeling and visualization of the IGSCC initiation and growth on the grain-size scale have already been proposed by the authors. Two essential features have been introduced in these algorithms: randomly oriented anisotropicaly elastic grains and embedded finite element solution of microscopic stress and strain fields. Main focus of the paper is given to the dependence of microscopic stress fields at crack tips on the random orientation of neighboring grains.

The incompatibility strains, which develop along the boundaries of randomly oriented anisotropic grains, are shown to influence the local stress fields at crack tips significantly. The limited number of calculations indicate that the anisotropic arrangement of grains with local incompatibility strains causes in average about 20% higher J-integral values at the crack tips than expected from the calculation in isotropic case.

More important consequence of incompatibility strains seems to be large variability of mode II contribution of J-integral. This implies that anisotropy could have extremely important impact on the direction of crack propagation. Further analysis is needed to quantify those effects more accurately.

1 INTRODUCTION

Intergranular stress corrosion cracking (IGSCC) of PWR steam generator tubes made of Inconel 600 has been the major cause of early retirement of PWR steam generators worldwide [2]. Significant efforts were devoted in the past to the assessment of reliability of affected tubes and to clarifications of main mechanisms governing the IGSCC.

The reliability aspects (see for example[5], [9] and references therein) provided valuable support in the maintenance of steam generators. However, the accuracy of the assessment was essentially limited by the ability of the available non-destructive examination methods to yield a meaningful and accurate "size" of detected crack networks. Better understanding of the defect development and morphology seems therefore to be the only way to improve the accuracy of the reliability estimates.

The identification and explanation of processes potentially responsible for the initiation and development of intergranular cracks were also topics of wide concern. But despite of a huge research performed in the past decades, the root mechanisms of IGSCC are still not understood completely [17]. Recent research shows that the IGSCC is dominated by the microstructural features, especially those on the grain boundaries [1].

Computational algorithms aiming at modeling and visualization of the IGSCC initiation and growth on the grain-size scale have already been proposed by the authors [8]. Randomness of the grain structure and of the crack initiation and growth processes were assumed. The random crack growth was simulated with algorithms allowing for crack branching, coalescence and interference. The method yielded patterns of cracks with shapes and structure comparable to those observed in experiments. However, a number of potentially important microscopic features (e.g., random orientation and anisotropy of grains, grain boundary mismatch etc.) were not taken into account. A convenient approximation with

isotropic continuum was implemented instead, allowing for simplified but efficient estimation of stress intensity factors.

In this paper, two essential features are introduced in the model: randomly oriented anisotropicaly elastic grains and embedded finite element solution of microscopic stress and strain fields. Main focus of the discussion is given to the dependence of local stress intensity factors on the random orientation of neighboring grains.

Potential of the proposed computational scheme with embedded commercially available finite element solvers to explicitly account for a variety of microstructural features (e.g., grain boundary mismatch characteristics etc.) is discussed in some detail.

2 MATHEMATICAL MODEL

The essential features of the proposed simulation procedure are described in this section, as follows:

- ☑ The random grain structure (in a plane) is modeled with Voronoi tessellation;
- ☑ Each grain is considered as anisotropic elastic monocrystal with randomly oriented material axes;
- ☑ The derivation of random crack shapes and
- ☑ The estimation of crack tip loading.

Discussion is closed with remarks on the current limitations and potential for future refinements of the method.

2.1 Voronoi Tessellation

A Voronoi tessellation represents a cell structure constructed from a Poisson point process by introducing planar cell walls perpendicular to lines connecting neighbouring points. This results in a set of convex polygons/polyhedra embedding the points and their domains of attraction, which completely fill up the underlying space. A survey about mathematical foundations and a variety of applications in different fields of science can be found for example in [19].

The concept of Voronoi tessellation has recently been extensively used in materials science, especially to model random microstructures like aggregates of grains in polycrystals, patterns of intergranular cracks and composites. Some examples of applications are calculation of properties of damaged polycrystals[3], characterization of fibre-reinforced composites [13], simulation of microcrack nucleation and propagation in creep [20], [4], thermal [15] and intergranular stress-corrosion [7]. All tessellations used in this paper were generated using the code VorTESS [18].

Only a subset of all Voronoi tessellations is suitable for finite element meshing with quadrilateral elements. For a discussion on necessary conditions and meshing algorithms see [22].

2.2 Anisotropic Elasticity

Each grain is assumed to be a **monocrystal** and behaves as randomly oriented anisotropic elastic continuum. It's consitutive law is therefore given by the generalized Hooke law [16]:

$$\sigma_{ij} = C_{ijkl} \cdot \varepsilon_{kl}\,, \qquad \textbf{Eq. (1)}$$

where σ_{ij} represents the second rank stress tensor, C_{ijkl} the fourth rank stiffness tensor and ε_{ij} the strain tensor. *i, j, k* and *l* are indices running from 1 to 3. Inconel 600 is a Ni-based alloy with face centered cubic (fcc) structure. This leads to three independent stiffness constants C_{iiii}=234.6 , C_{iijj}= 145.4 and C_{ijij}= 126.2 GPa [12]. Isotropic continuum is fully described by

only two stiffness constants. In this example, Young's modulus of 210 GPa and Poisson ratio of 0.3 were assumed.

The elastic properties (e.g., stiffness and compliance tensor) of the **polycrystalline aggregate** are completely defined by the properties of and interaction between the monocrystals. The standard procedure for the estimation of the overall macroscopic behavior of interacting monocrystals is to average the stress and strain tensors over all material directions and over the volume [16]. The volume averaged stress $<\sigma_{ij}>$ and strain tensors $<\varepsilon_{kl}>$ may be used to estimate the equivalent (macroscopic) stiffness C^*_{ijkl} or compliance D^*_{ijkl} tensors:

$$\left\langle \sigma_{ij} \right\rangle = C^*_{ijkl} \left\langle \varepsilon_{kl} \right\rangle ,. \qquad \textbf{Eq. (2)a}$$

$$\left\langle \varepsilon_{kl} \right\rangle = D^*_{ijkl} \left\langle \sigma_{ij} \right\rangle . \qquad \textbf{Eq. (2)b}$$

Please note that for an arbitrary polycrystalline aggregate the inverse compliance tensor does not necessarily equal to the stiffness tensor

$$C^*_{ijkl} \neq \left(D^*_{ijkl} \right)^{-1} . \qquad \textbf{Eq. (3)}$$

In fact, the different behavior of both tensors is governed by the size of the aggregate and macroscopic boundary conditions [16]: solution of Eq. (2)a therefore assumes prescribed macrostress, while Eq. (2)b assumes prescribed macrostrain.

The differences between the stress and compliance tensors tend to vanish with increasing number of grains in the polycristalline aggregate. The aggregate satisfying the property

$$C^*_{ijkl} \cong \left(D^*_{ijkl} \right)^{-1} \qquad \textbf{Eq. (4)}$$

is called the **Representative Volume Element (RVE)**. In general, large enough RVE will satisfy any boundary conditions.

The microstress and microstrain fields are obtained using commercially available finite element solver ABAQUS [11]. Grains are fully coupled together at the intact grain boundaries.

2.3 Positions and Shapes of Cracks

The random crack shapes strictly follow the grain boundaries and always extend completely over boundary between two or more grains. All crack shapes in this paper were derived using random crack initiation and growth processes, described in [16].

It should be noted that the random crack growth process in [16] is substantially supported by the empirical estimates of the stress intensity factors at crack tips, which are fully described in [15]. Those estimates are in principle very accurate for simple (e.g., straight) cracks and may loose accuracy with increasing complexity of the crack shape [14].

2.4 Crack Tip Loading

The loading of the crack tips is achieved through the prescribed macroscopic remote biaxial stress field. The J-integrals are then calculated for each crack tip using the built–in features of ABAQUS [11]. Further, the ABAQUS results were post-processed to decompose the J-integral on mode I and mode II contributions [14]. This decomposition is essential for the determination of preferred crack propagation direction from the observed crack tip, which is always located in a triple point.

The scatter caused by the randomly shaped finite element meshes at different crack tips has been studied in isotropic continuum and reported as reasonable elsewhere [14].

For the verification purposes, the straight crack is approximated by an inclined crack in an isotropic infinite plane [10], expressing the stress intensity factors in mode I and II as:

$$K_I = \frac{\sigma \cdot \sqrt{\pi \cdot a}}{2}\left[(1+k)-(1-k)\cdot\cos(2\cdot\alpha)\right] \text{ and} \qquad \textbf{Eq. (5)}$$

$$K_{II} = \frac{\sigma \cdot \sqrt{\pi \cdot a}}{2}\left[(1-k)\cdot\sin(2\cdot\alpha)\right]. \qquad \textbf{Eq. (6)}$$

The crack is assumed to be parallel to the x axis. Mode I is therefore driven by σ_{yy}. The x axis is inclined against second principal stress (σ_{22}) by angle α. The ratio between the principal stresses is denoted by k ($\sigma_{11} = k\ \sigma_{22} = k\ \sigma$). Corresponding J-integral values for both loading modes (J, J_I and J_{II}) are obtained as:

$$J_i = \frac{K_i^{\,2}}{E'}, i = \{I, II\} \quad \rightarrow \quad J = J_I + J_{II}, \qquad \textbf{Eq. (7)}$$

where E' represents Young's modulus E in plane stress and $E/(1-\upsilon)^2$ in plain strain. υ is Poisson's ratio.

2.5 Main Limitations and Potential of the Proposed Approach

Currently available computational capabilities suggest limitation of the analysis to 2-D (plane stress, plane strain, generalized plane strain). Some extrapolations towards full 3-D analysis may be obtained by independent 2-D analyses in planes perpendicular to each other [16]. Extension of the method to 3-D is nevertheless straightforward, pending development in computational capabilities.

The grain boundaries are currently used for only two purposes: as a limit between grains with different orientations of material axes and as potential path of intergranular cracks. An obvious application to be added in the near future is calculating the grain boundary mismatch. This will enable assigning different failure probabilities to high and low angle boundaries, which show (for example) significantly different amount of interganular carbides [1]. Another future application deserving closer attention is to implement crystal plasticity or similar models of inelastic deformation to gain more realistic insights in the microscopic stress and stress fields and consequently also in the behavior of short cracks.

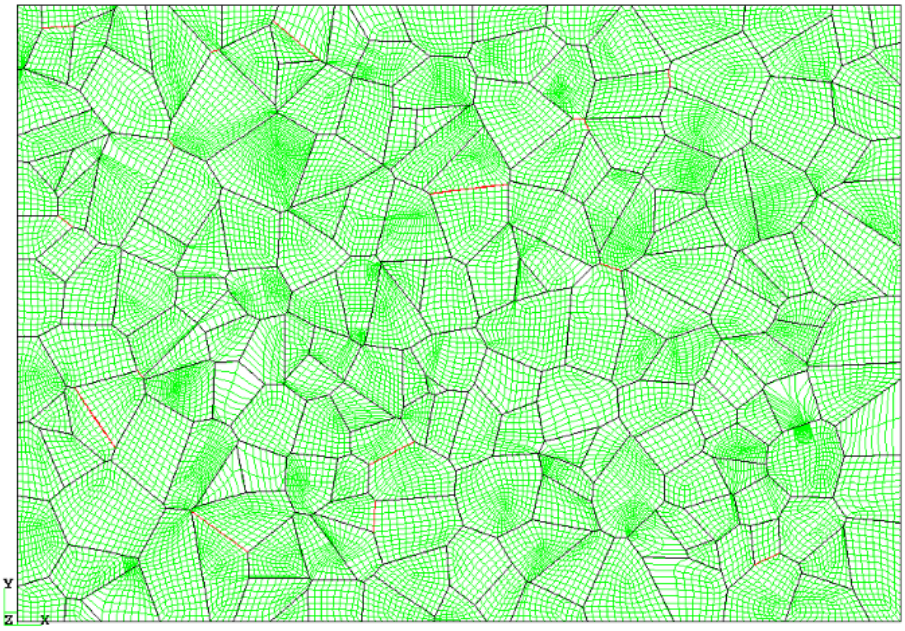

Figure 1 Finite element mesh of the simulated random grain structure. Remote loading by tensile stress of 2 MPa in X and 1 MPa in Y direction. Cracked grain boundaries are

plotted in red.

3 NUMERICAL EXAMPLE

3.1 Models

The random grain structure was realized using the Voronoi Tesselation (code VorTESS [18]). The planar structure with 201 grains is depicted in Figure 1 with black lines representing the intact grain boundaries and red lines representing cracked grain boundaries. The size of the window is, assuming average grain size of about 30 μm, approx. 0.5 by 0.3 mm.

The finite element mesh used in subsequent calculations is depicted in Figure 1, too. The loading of the mesh is prescribed tensile macrostress with magnitudes 2 and 1 MPa in X and Y directions, respectively. The displacement boundary conditions are chosen appropriately to prevent rigid body motion of the investigated structure.

Two distinct cases are studied: (1) isotropic elastic continuum with grain boundaries used only to model the potential and actual crack paths and (2) polycrystalline aggregate with grains modeled as randomly oriented anisotropic continua. In both cases, the microstress field and the influence of randomly oriented grains on the magnitude and orientation of the crack tip loading are sought.

3.2 Microscopic stress fields

The von Mises equivalent stress obtained assuming the isotropic continuum is shown in Figure 2. The cracked grain boundaries are plotted in bold black lines. The stress singularities at the crack tips behave as predicted by linear elastic fracture mechanics and are clearly seen from Figure 2. Also, some limited intereference between cracks may be seen. However, this is not the primary concern of this paper.

The randomly oriented anisotropic grains tend to develop significantly different distribution of von Mises equivalent stress (Figure 3). It is clearly seen that the incompatibility stresses/strains which develop along the essentially incompatible grain boundaries dominate the development of the microscopic stress field. It should be noted however that only one particular realization of the random grain structure is leading to the stress distribution depicted in Figure 3. Other realizations may lead to different distributions. Large variations of strain energy stored in the system are however not expected.

A close-up look at the largest crack in the system (black rectangle in Figure 2 and Figure 3) is comparatively shown for this crack in isotropic (Figure 4) and two different realizations of anisotropic material (Figure 5). The incompatibility strains which develop along the grain boundaries significantly influence the local stress fields at crack tips. The level and directions of disturbances seem to depend strongly on the orientation of neighboring grains (denoted as local coordinate systems in Figure 4 and Figure 5), which is an expected result. Again, the areas affected by the stress concentrations at crack tips do not seem to vary significantly.

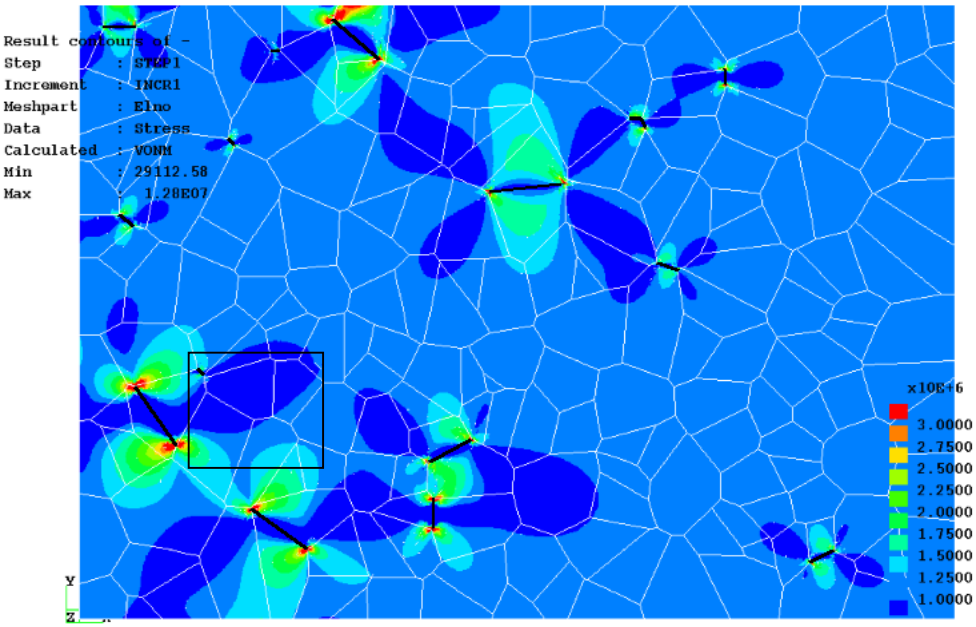

Figure 2 Von Mises equivalent stress (isotropicaly elastic continuum, Pa)

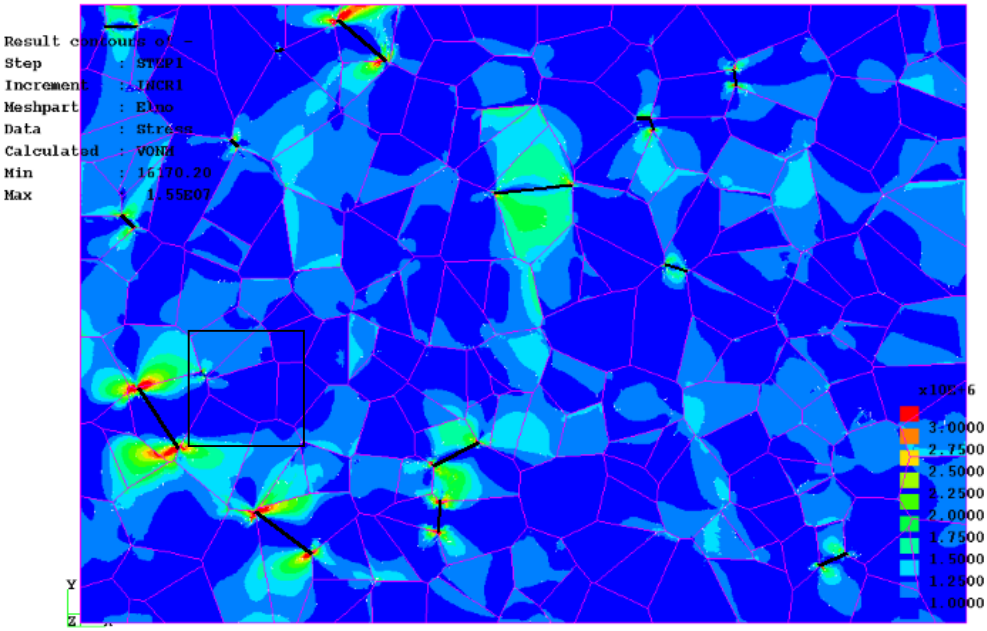

Figure 3 Von Mises equivalent stress (anisotropicaly elastic grains with random material orientations, Pa)

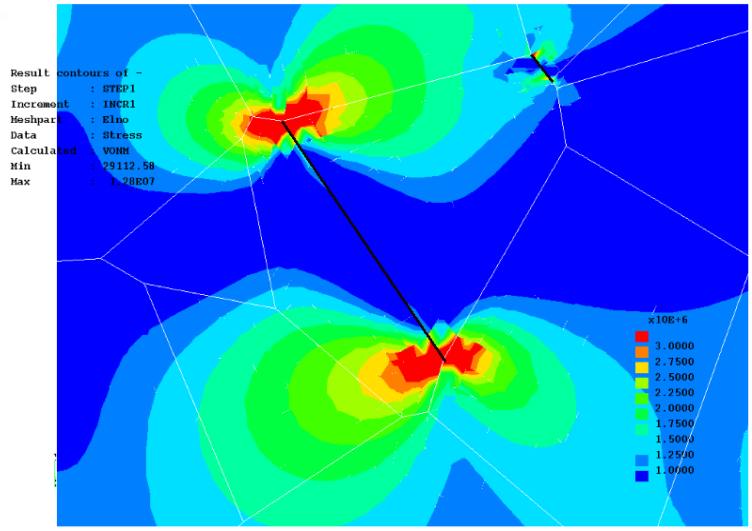

Figure 4 Von Mises equivalent stress in the vicinity of crack tip- Isotropic continuum (macro location denoted by squares in Figure 2 and Figure 3)

3.3 J-Integrals

The scatter of J-integral values obtained from the isotropic and anisotropic model has been studied in some detail to obtain further measures of the variability of microscopic stress fields in the vicinity of crack tips. Ten different realizations of random orientation were used for this purpose. The arrangements of grains was not changed: contribution from different arrangements of grains (e.g., tessellations) was found to be statistically less important that variations in material orientations [21].

The stability and mesh-dependence of numerical J-integral estimates and their decomposition to the mode I and mode II contributions in the isotropic case have been studied and reported upon elsewhere [14]. Comparison of different numerical methods estimating the local stress fields at crack tips, reported elsewhere [6], additionally confirmed numerical stability and accuracy of the method used.

Figure 6 depicts the scatter of anisotropic J-integral values as a function of crack length. The scatter seems to be virtually independent of crack length (It should be noted here that larger numerical error is expected for shorter cracks with potentially limited number of available independent contours for the calculation of J-integrals [14]). Other expected observation is the fact that the anisotropic arrangement of grains with local incompatibility strains causes in average some 20% more loading on the crack tips than expected from the calculation in isotropic case. Further analysis is needed to quantify this effect more accurately.

The biaxiality of loading and inclination of cracks against the remote macroscopic principal stresses causes significant contribution from the mode II loading. In the isotropic case, the value of J_I is typically of the same order of magnitude as J, while J_{II} typically assumes about up to 10% of the value of J_I. Larger scatter in J_{II} is therefore to be expected and was confirmed (see Figure 7).

The scatter in J_{II} is depicted in Figure 7 as a function of crack inclination against the global x-axis of the model Figure 1. Crack length and inclination are the only sources of variability in J_{II} in the isotropic case (see Eq. (6)). Both of them were kept fixed in the simulation, which points the anisotropy (and potential numerical errors!) the only source of variability in Figure 7. This implies that anisotropy could have extremely important impact on the direction of crack propagation. The results obtained to date do not support any correlation between scatter of J_{II} and the crack inclination axes.

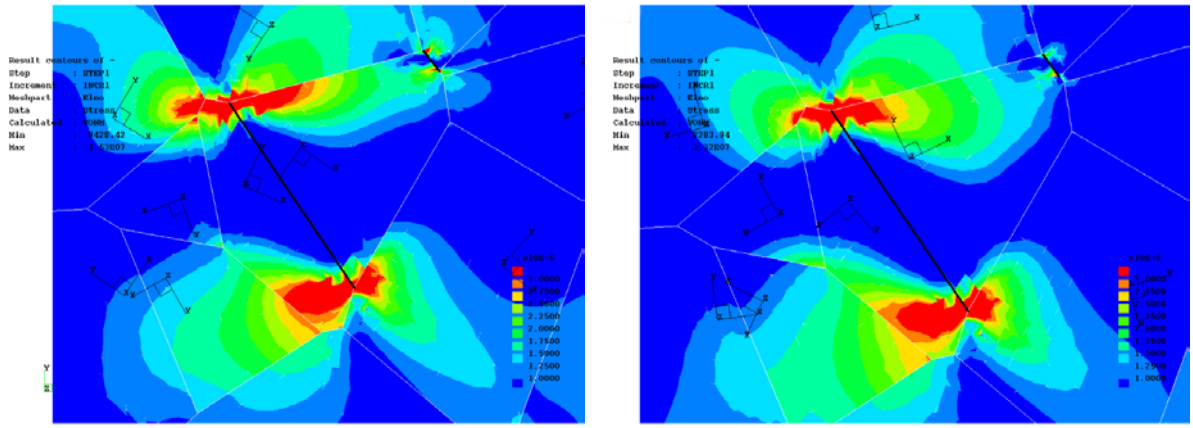

Figure 5 Von Mises equivalent stress in the vicinity of crack tip-different realizations of randomly oriented anisotropic continua (macro location denoted by squares in Figure 2 and Figure 3)

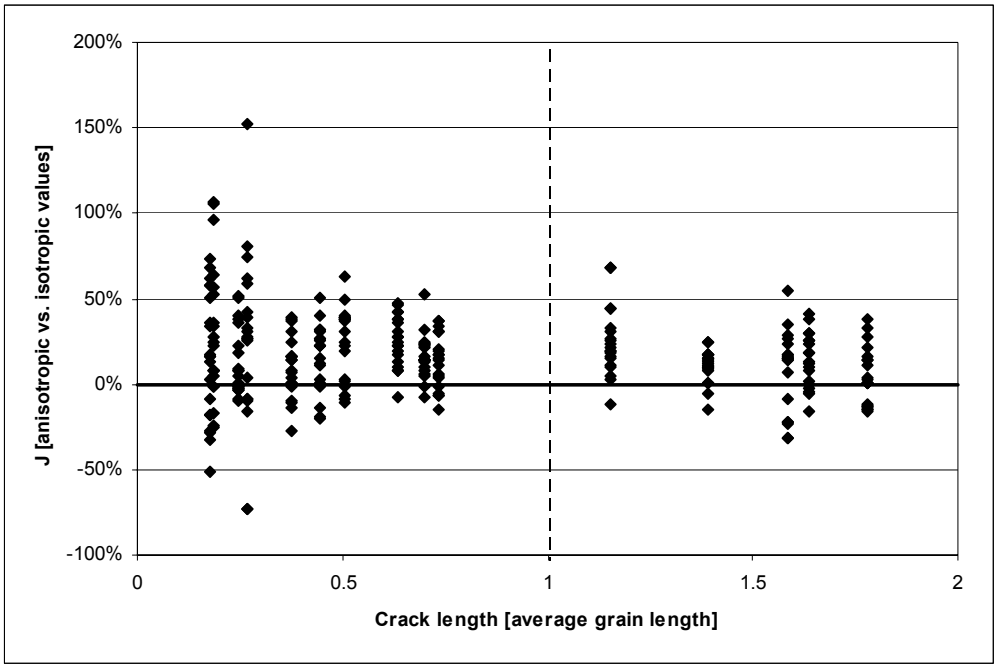

Figure 6 Scatter of "anisotropic" J-integral values obtained from finite element solution (0 obtained from isotropic finite element solution).

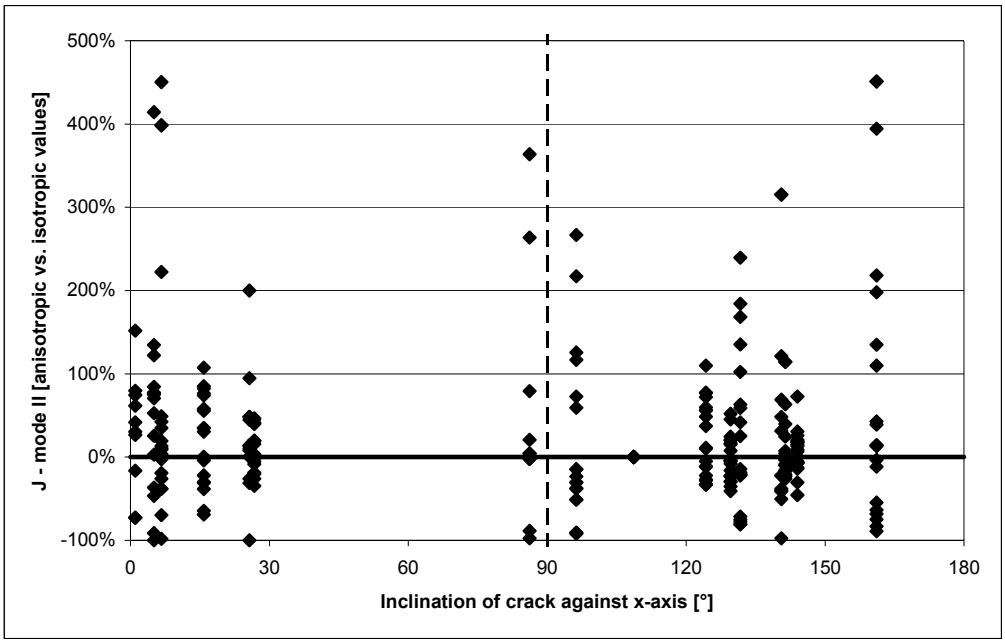

Figure 7 Scatter of "anisotropic" mode II J-integral values obtained from finite element solution (0 obtained from isotropic finite element solution).

4 CONCLUSIONS

Computational algorithms aiming at modeling and visualization of the IGSCC initiation and growth on the grain-size scale have already been proposed by the authors. Two essential features have been introduced in these algorithm: randomly oriented anisotropicaly elastic grains and embedded finite element solution of microscopic stress and strain fields.

The incompatibility strains which develop along the boundaries of randomly oriented anisotropic grains significantly influence the local stress fields at crack tips. The limited number of calculations indicate that the anisotropic arrangement of grains with local incompatibility strains causes in average about 20% higher J-integral values at the crack tips than expected from the calculation in isotropic case.

More important consequence of incompatibility strains seems to be large variability of mode II contribution of J-integral. This implies that anisotropy could have extremely important impact on the direction of crack propagation. Further analysis is needed to quantify those effects more accurately.

Potential of the proposed computational scheme with embedded commercially available finite element solvers to explicitly account for a variety of microstructural features (e.g., grain boundary mismatch characteristics etc.) in the future is discussed.

5 ACKNOWLEDGEMENTS

This work was supported by the Ministry of Science of Republic of Slovenia through the Programme-106-505. The authors are also indebted to Dr. H. Riesch-Oppermann of Forschungszentrum Karlsuhe, Germany, and Dr. Stefan Weyer of University of Karlsruhe, Germany, for numerous discussions.

6 REFERENCES

[1] Alexandreanu B, Capell B, Was GS. Combined effect of special grain boundaries and grain boundary carbides on IGSCC of Ni-16Cr-9Fe-xC alloys. Materials Science and Engineering A 2001; 300(1-2):94-104.

[2] Banic MJ, Bros J, Cizelj L *et al.* Assessment and Management of Ageing of Major Nuclear Power Plant Components Important to Safety: Steam Generators. Vienna, Austria: International Atomic Energy Agency, IAEA-TECDOC-981, 1997:1-173. IAEA Safety Series.

[3] Brückner-Foit A, Weyer S. Overall Properties of Ceramics Subjected to Compressive Loading. International Conference on Engineering Ceramics and Structures. 2000.

[4] Cannmo P. An Interface Model Based on Damage Coupled to Slip and Dilatation. Proceedings of the 12th Bienniel Conference on Fracture-ECF 12. 1998: 957-62.

[5] Cizelj L, Hauer I, Roussel G, Cuvelliez C. Probabilistic Assessment of Excessive Leakage through Steam Generator Tubes Degraded by Secondary Side Corrosion. 185. 1998:347-59.

[6] Cizelj L, Kovše I. Short Intergranular Cracks in the Piecewise Anisotropic Continuum Model of the Microstructure. Jenèiè I, Glumac B. International Conference "Nuclear Energy in Central Europe 2001", Proceedings. Ljubljana, Slovenija: Nuclear Society of Slovenia, 2001.

[7] Cizelj L, Riesch-Oppermann H. Modeling the Early Development of Secondary Side Stress Corrosion Cracks in Steam Generator Tubes Using Incomplete Random Tessellation. Chang SP. Transactions of the 15th International Conference on Structural Mechanics in Reactor Technology (SMiRT 15). V. 1999:V-217-V-224.

[8] Cizelj L, Riesch-Oppermann H. Modeling the Early Development of Secondary Side Stress Corrosion Cracks in Steam Generator Tubes Using Incomplete Random Tessellation. Nuclear Engineering and Design 2001; in printing.

[9] Dvoršek T, Cizelj L, Mavko B. Safety and Availability of Steam Generator Tubes Affected by Secondary Side Corrosion. 185. Amsterdam: Elsevier Science, 1998:11-21.

[10] Eftis J, Jones DL, Liebowitz H. Load biaxiality and fracture: Synthesis and summary. Engineering Fracture Mechanics 1990; 36(4):537-74.

[11] Hibbit K&SI. ABAQUS/Standard User's Manual, Version 5.8. Pawtucket, R.I., USA: Hibbit, Karlsson & Sorensen Inc., 1998.

[12] Holden TM, Holt RA, Tomé CN. Intergranular strains in Inconel-600. Materials Science and Engineering A 2000; 131-6.

[13] Johansson T. Analytische Beschreibung von Experimenten an fäserverstärkten Keramiken zur Bestimmung von Grenzflächenparametern. Vol. VDI Reihe 18, No. 170. Düsseldorf, Germany: VDI Verlag, 1995.

[14] Kovač M, Cizelj L. Numerical Analysis of Interacting Cracks in Biaxial Stress Field. Proc of Int Conf Nuclear Eergy in Central Europe. 1999: 259-66.

[15] Kullig E, Johansson T, Brückner-Foit A *et al*. Ermittlung der Lebensdauerverteilung bei Thermoermüdung mit der Methoden der Stochastischen Geometrie. Karlsruhe, Germany: Forschungszentrum Karlsruhe, 1996; FZK-5692.

[16] Nemat-Nasser S. Overall Stresses and Strains in Solids with Microstructure. Gittus J, Zarka J. Modelling Small Deformations of Polycrystals. London: Elsevier, 1986: 41-64.

[17] Rebak RB, Szklarska-Smialowska Z. The mechanism of stress corrosion cracking of Alloy 600 in high temperature water. Corrosion Science 1996; 38(6):971-88.

[18] Riesch-Oppermann H. VorTess, Generation of 2-D random Poisson-Voronoi Mosaics as Framework for the Micromechanical Modelling of Polycristalline Materials. Karlsruhe, Germany: Forschungszentrum Karlsruhe, 1999; Report FZKA 6325.

[19] Stoyan D, Kendall WS, Mecke J. Stochastic Geometry and its Applications. Chichester, England: John Wiley & Sons, 1995.

[20] Van der Giessen E, Tvergaard V. Development of Final Creep Failure in Polycrystalline Aggregates. Acta Metall. Materialia 1994; 42(3):959-73.

[21] Weyer S. Experimentelle untersuchung und mikromechanische Modellierung des Schädigungsverhaltens von Aluminiumoxid unter Druckbeanspruchung Karlsruhe, Germany: Universität Karlsruhe, 2001.

[22] Weyer S, Fröhlich A, Riesch-Oppermann H, Cizelj L, Kovač M. Automatic Finite Element Meshing of Planar Voronoi Tessellations. Submitted to Engineering Fracture Mechanics 2000.